Journal of Aerosol Science 48 (2012) 18–33

Contents lists available at SciVerse ScienceDirect

Journal of Aerosol Science

journal homepage: www.elsevier.com/locate/jaerosci

Experimental determination of deposition of diesel exhaust particles in the human respiratory tract

Jenny Rissler [a,*], Erik Swietlicki [b], Agneta Bengtsson [b], Christoffer Boman [c], Joakim Pagels [a], Thomas Sandström [d], Anders Blomberg [d], Jakob Löndahl [a,b]

[a] Ergonomics and Aerosol Technology, Lund University, P.O. Box 118, SE-221 00, Lund, Sweden
[b] Division of Nuclear Physics, Lund University, P.O. Box 118, SE-221 00, Lund, Sweden
[c] Energy Technology and Thermal Process Chemistry, Umeå University, SE-901 87, Umeå, Sweden
[d] Department of Public Health and Clinical Medicine, Division of Medicine/Respiratory Medicine, Umeå University, SE-901 87 Umeå, Sweden

ARTICLE INFO

Article history:
Received 19 October 2011
Received in revised form
16 January 2012
Accepted 17 January 2012
Available online 26 January 2012

Keywords:
Diesel exhaust
Particle
Agglomerates
Lung deposition
Dose
Surface area

ABSTRACT

Diesel emissions are a major contributor to combustion-generated airborne ambient particles. To understand the role of diesel particulate emissions on health effects, it is important to predict the actual particulate dose deposited in the human respiratory tract, with respect to number, surface area and mass. This is complicated by the agglomerate nature of some of these particles. In this study the respiratory tract deposition fraction in the size range 10–500 nm, was determined for 10 healthy volunteers during both idling and transient engine running conditions of a heavy duty diesel engine. The aerosol was characterized with respect to both chemical and physical properties including size resolved particle effective density. The dominating part of the emitted particles had an agglomerate structure. For those formed during transient running conditions, the relationship between particle mass and mobility diameter could be described by a power law function. This was not the case during idling, most likely because of volatile compounds condensing on the agglomerates. The respiratory tract particle deposition revealed large intra-subject variability with some subjects receiving a dose that was twice as high as that of others, when exposed to the same particle concentration. Associations were found between total deposited fractions (TDF), and breathing pattern. There was a difference between the idling and transient cycle with TDF being higher with respect to number during idling. The measured size-dependent deposition fraction of the agglomerated exhaust particles from both running conditions was nearly identical and closely resembled that of spherical hydrophobic particles, if plotted as a function of mobility diameter. Thus, for the size range covered, the mobility diameter could well describe the diameter-dependent particle respiratory tract deposition probability, regardless of the agglomeration state of the particles. Whilst mobility diameter well describes the deposition fraction, more information about particle characteristics is needed to convert this to volume equivalent diameter or estimate dose with respect to surface area or mass. A methodology is presented and applied to calculate deposited dose by surface area and mass of agglomerated particles. The methodology may be useful in similar studies estimating dose to the lung, deposition onto cell cultures and in animal studies.

© 2012 Elsevier Ltd. All rights reserved.

* Correspondence to: Division of Ergonomics and Aerosol Technology, Department of Design Sciences, P.O. Box 118, SE-221 00, Lund, Sweden. Tel.: +46 46 2220534; mobile: +46 70 1518426; fax: +46 46 2224709.
E-mail address: jenny.rissler@design.lth.se (J. Rissler).

0021-8502/$ - see front matter © 2012 Elsevier Ltd. All rights reserved.
doi:10.1016/j.jaerosci.2012.01.005

Nomenclature

a_k,b_k, c_k, d_k	Fitted parameters for describing measured deposition fraction (Eq. (7))
APM	aerosol particle mass analyzer
B	mechanical mobility
C_c	Cunningham correction term
C_{ex}	exhaled particle concentration
C_{in}	inhaled particle concentration
CPC	condensation particle counter
D	particle diffusivity
d	particle diameter
DEP	diesel exhaust particles
$DF(d)$	size-resolved deposited fraction in the respiratory tract
DF_{equip}	instrumental particle losses in RESPI
DMA	differential mobility analyzer
d_{me}	particle electrical mobility equivalent diameter
d_{pp}	primary particle diameter
EC	elemental carbon
f	breathing frequency
FVC	forced vital capacity
GMD	geometric mean diameter
k	Boltzmann constant
K	parameter fitted describing the mass–mobility relation of the particles (Eq. (3))
m	particle mass
m_{agg}	mass of individual agglomerates
MV	minute volume
N	particle number
N_{agg}	number of agglomerates
N_{pp}	number of primary particles
OC	organic carbon
PAH	polycyclic aromatic hydrocarbon
Q	inhaled volume flow
s.d.	standard deviation
SA	surface area
SA_{agg}	surface area of individual agglomerates
SA_{sph}	surface area of spherical particles
SMPS	scanning mobility particle sizer
t	exposure time
T	temperature
TC	total carbon
TD	thermo-denuder
TDF_m	total deposited fraction in the respiratory tract with respect to particle mass
TDF_N	total deposited fraction in the respiratory tract with respect to particle number
TDF_{SA}	total deposited fraction in the respiratory tract with respect to particle surface area
TEM	transmission electron microscopy
TEOM	tapered element oscillating microbalance instrument
V_D	instrumental dead space
V_T	tidal volume
η	kinematic viscosity of air
ρ_{eff}	effective density
ε_m	mass–mobility exponent
ρ_{pp}	density of the primary particles
σ_g	geometric standard deviation

1. Introduction

Air pollution has been associated with a variety of adverse health effects (Pope & Dockery, 2006) and is believed to be one of the major causes of premature deaths worldwide (Lopez et al., 2006). Particles emitted from combustion processes, whereof diesel engines are a major contributor, are among the most common emissions in populated areas. Epidemiological and toxicological studies have shown associations between diesel exhaust and adverse health effects (e.g. Hart et al., 2009; Mills et al., 2007; Sydbom et al., 2001). Experimental exposure studies of humans have revealed that exposure to dilute diesel exhaust induces a pronounced neutrophilic airway inflammation along with negative cardiovascular effects in terms of reduced vasomotor function and impaired endogenous fibrinolysis (Salvi et al., 1999; Mills et al. 2005; Mills et al., 2007; Barath et al., 2010). Whilst recent research efforts have provided a basis for better understanding of exposure, deposition, uptake and kinetics, the mechanisms behind the health effects are far from fully understood.

The exhaust from diesel engines includes several air pollution components such as ultrafine soot particles, smaller nucleation mode particles, nitrogen oxides, a range of organic compounds including polycyclic aromatic hydrocarbons (PAHs) and oxy-PAHs, and metal emissions, all of which are believed to play an important role in the observed health effects caused by ambient aerosols (Sydbom et al., 2001; Maricq, 2007). A key link between exposure to diesel emissions and the health response is the respiratory tract deposition of inhaled particles. So far, respiratory tract deposition has predominantly been investigated for spherical, hydrophobic and monodisperse particles, and only few experimental studies have investigated the deposition of real-world aerosols, such as combustion exhaust particles, which may be agglomerated, non-hydrophobic and almost always polydisperse (Maricq & Xu, 2004; Rissler et al., 2005, 2006). Furthermore, more lung deposition data are needed as the large intra-subject variability is not captured by models (Hofmann, 2011).

Measurements of respiratory tract deposition of aerosols emitted during combustion, other than tobacco smoke, are scarce (Löndahl et al., 2008, 2009; Morawska et al., 2005). Löndahl et al. (2008, 2009) have shown that hygroscopicity indeed alters particle lung deposition substantially. Morawska et al. (2005) examined deposition of particles from diesel and petrol combustion in 14 healthy non-smoking young adults. The deposition partly deviated from model predictions and hygroscopicity was suggested as the main explanation. Another suggested explanation was particle morphology. The hygroscopic growth, chemical composition or effective density of the particles was, however, not provided in that study.

Diesel exhaust particles (DEP) typically consist of two modes: a soot dominated accumulation mode with a geometric mean diameter (*GMD*) of around 50–90 nm, and a smaller nucleation mode (Maricq, 2007). If, as in the present study, the exhaust particles originate from combustion of a modern diesel fuel with low sulphur content, fresh diesel exhaust particles are nearly hydrophobic (Weingartner et al., 1997, 2002). Other types of combustion-generated particles, such as those from biomass combustion, may be highly hygroscopic (Rissler et al., 2005). When it comes to the toxicological effects of DEP and to distinguish their chemical and physical properties, their volatile and non-volatile content, as well as solubility, are important aspects (Giechaskiel et al., 2009). Another important property of fresh diesel exhaust particles is that they most often are porous and highly agglomerated and aggregated (Maricq & Xu, 2004; Park et al., 2003). Agglomerates and aggregates are in this publication referred to as agglomerates, including inter-particle bond energies ranging from weak van-der Waals forces to stronger solid-state necks.

The particle size determination is often made using a Differential Mobility Analyzer (DMA). Despite the complex particle shape of agglomerates, sizing of particles according to their mobility diameter (as when using a DMA) is expected to describe the deposition probability in the respiratory tract for the size fraction where diffusion is the dominating deposition mechanism (Schmid et al., 2008). Although the deposition due to diffusion may be modeled with reasonable accuracy using the mobility equivalent diameters, the fractal nature of particles does introduce additional uncertainties into model predictions (Hofmann, 2011). It was demonstrated in one study using a cast of a section of a human lung (generation 3–9) that agglomerated particles have an increased deposition probability due to interception in regions where gas flow undergoes transitions (Scheckman & McMurry, 2011). DEP mainly consists of particles below 400 nm which are, to a great extent, expected to deposit in the pulmonary region (Alföldy et al., 2009). Hence, the deposition of an agglomerated aerosol, such as diesel exhaust and many types of engineered nanoparticles, in the human lungs is still unclear.

Even if mobility diameter is argued to be a good measure of the size-dependent deposited fraction, it is far from a complete metric for deposited surface area or mass dose, as pointed out in a modeling study by Broday & Rosenzweig (2011). In order to estimate deposited surface area or mass dose from number size distributions measured by mobility analyzers that incorporate DMA-techniques (SMPS, FMPS, EEPS, DMS, TDMA, etc.), more information such as particle shape and the relationship between mobility diameter and agglomerate particle mass (effective density) is needed.

The objective of this research is to determine respiratory tract deposition in healthy humans of two different types of DEP, and to compare this with previous deposition measurements of spherical particles, carried out using the same methodology. The characterization of diluted exhaust particles with respect to agglomeration, effective density and composition was also performed to enable a discussion of the relation between the determined respiratory tract deposition and detailed physicochemical particle properties. Furthermore, an estimation of deposited mass is presented, separated into volatile and non-volatile fractions. Finally, a model to estimate the surface area of the deposited agglomerates from the measured deposition fraction and the physical characteristics of the particles is presented and applied.

2. Methods

2.1. Particle respiratory tract deposition measurements

The respiratory tract deposition measurements were performed using a previously developed set-up (RESPI), which was comprehensively described by Löndahl et al. (2006) and used in several previous studies (Löndahl et al., 2007, 2008, 2009). Fig. 1 shows a schematic diagram of the set-up. The measurements were performed during normal tidal breathing through a mouthpiece, wearing a nose clip, while sitting in a relaxed position. The breathing pattern was monitored on-line.

Briefly, the dry ($<20\%$ RH) particle size distribution was measured with a Scanning Mobility Particle Sizer (SMPS), sampling alternately from the inhaled and exhaled air. The size range covered was 10–500 nm. The deposition fraction as

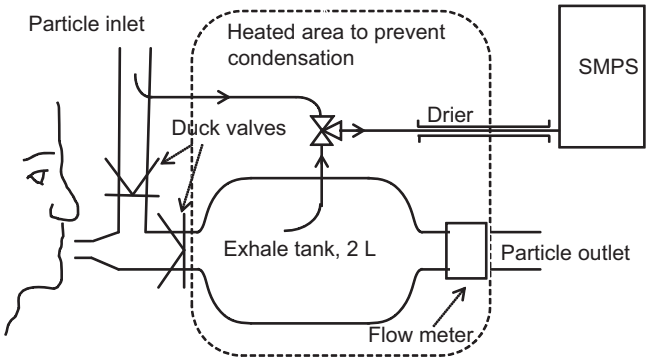

Fig. 1. Schematic diagram of the RESPI set-up. The inhaled air is drawn from the particle inlet, connected to the exposure chamber. Exhaled air is directed by one-way duck valves into the exhale tank.

a function of particle diameter (DF_{meas}) was determined by comparing the particle number concentration in each size bin from the SMPS of exhaled vs. inhaled air (Fig. 1).

To estimate the true size-resolved deposited fraction ($DF(d_{me})$), corrections to DF_{meas} were made for (*i*) instrumental particle losses, DF_{equip}, (Löndahl et al., 2006), and (*ii*) instrumental dead space, V_D, (Gebhart et al., 1989; Löndahl et al., 2007). These corrections were made individually for each subject and each session as they depend on the breathing pattern according to

$$DF(d_{me}) = \frac{V_T}{V_T - V_D}\left(1 - \frac{C_{ex}(d_{me})}{C_{in}(d_{me})(1 - DF_{equip}(d_{me}))}\right) \quad (1)$$

where V_T is the tidal volume, d_{me} electrical mobility particle equivalent diameter, C_{in} measured inhaled particle concentration, and C_{ex} measured exhaled particle concentration.

2.1.1. Measurement procedure

The measurements were performed on two different types of diluted diesel exhaust, one generated during idling and one during transient engine running conditions. These are described further in Sections 2.3 and 3.1. Each measurement session consisted of three exposure periods: one 3-min test period during which the subject became familiarized with the set-up and the equipment was checked, followed by two 15-min periods during which the deposition was measured. The same procedure was repeated for the two types of diesel exhaust for each subject, although on different days.

2.2. Subjects

The subjects participating in the study were 10 healthy volunteers (5 men and 5 women), aged 23–45. All were non-smokers with normal lung function (> 80% of predicted, see appendix, Table A1). Age, sex, breathing parameters and lung function of the individual subjects are provided in Table A1. Average values and standard deviations (s.d.) are given in Table 1. One of the male subjects was excluded from the evaluation as his breathing pattern (f=4.5 breaths/min, V_T=2.5 L) was considered forced. The study protocol was approved by the local ethics committee and an informed written consent was obtained from all subjects.

SPSS (SPSS Inc., IBM Corporation, version 19) was used to carry out the statistical analysis. The correlation analysis was calculated with Pearson's product moment and significances of differences between means were calculated with Student's *t*-test. The significances considered were at the 0.05 or 0.01 levels.

2.3. Aerosol generation and measurement conditions

Subjects were exposed to DEP generated by a diesel engine (Volvo TD40 GJE, 4.0 L, four cylinders, 1996) with no exhaust after-treatment, operated on a Volvo standard diesel fuel (SD-VSD-10). The specification of the Volvo diesel fuel is similar to the European automotive standard diesel (EN590) with a sulfur content of 5–7 mg/kg and PAH content of 2–6% by mass. The engine was operated in a motor test bench with a computer-controlled engine dynamometer that enabled simulation of the two experimental engine running conditions: idling and transient. Transient operating conditions (i.e. varying load and speed) were constituted according to the standardized test protocol of the urban part of the European Transient Cycle (Barath et al., 2010). A partial exhaust flow was selected and diluted in two steps with clean air in a procedure to mimic ambient conditions, and thereafter introduced into a human exposure chamber from where the subsequent sampling to the RESPI set-up was performed. The primary dilution ratio was 10–15 times by introducing the partial exhaust flow, driven by overpressure, in a mixing/residence chamber (L=600 mm, D=60 mm) that enabled a residence time of 1–3 s before the second dilution step. A total dilution ratio (i.e. raw exhaust gas to chamber) was approximately 100–150 times during idling conditions and 200–450 times during the transient cycle. The condition in the chamber was continuously monitored in terms of temperature, CO and NO_x gases, as well as particle (PM_{10}) mass concentration. The set-up and test procedures are further described in detail elsewhere (Barath et al., 2010; Lucking et al., 2011).

Table 1
Values in parentheses are percent of predicted value (pp). V_T denotes tidal volume, f breathing frequency, VC vital capacity and FEV_1 forced expiratory volume in the first second of exhalation. V_T and f were measured during the RESPI measurements.

Subject	Gender (M/F)	Age (yr)	Height (cm)	Weight (kg)	V_T (L)	f (min^{-1})	VC (pp) (L)	FEV_1 (pp) (L)
Mean	4/5	31.6	170	65.5	0.86	10.3	4.67(109)	3.98(109)
s.d.		8.4	10	7.9	0.34	3.6	1.1(13)	1.1(12)

2.4. Aerosol characterization

2.4.1. Mass concentration and carbon analysis

The mass concentration of the diluted DEP in the chamber was monitored by an on-line Tapered Element Oscillating Microbalance instrument (TEOM 1400) operated at 50 °C and equipped with a PM_{10} inlet. In addition, standard filter sampling for the gravimetrical determination of PM_{10} mass concentration was performed. The carbonaceous material in the diluted DEP in the chamber was characterized in terms of organic carbon (OC) and elemental carbon (EC). Samples for the OC/EC analysis was taken during the RESPI campaign using quartz and teflon+quartz filters in parallel (Wierzbicka et al., 2005) and subsequently analyzed using a thermal–optical carbon analysis method (NIOSH 5040).

2.4.2. Particle number size distribution

The particle number size distribution was measured using an SMPS built into the RESPI. It consisted of a bipolar charger, a custom built Differential Mobility Analyzer (DMA) of Vienna type (length 28 cm, inner/outer radius 25/32.4 mm, aerosol flow rate 1 l/min and sheath flow rate 10 l/min) covering the particle size range of 10–500 nm. The SMPS (and other mobility analyzers such as FMPS and DMS500) characterizes the particles according to their electrical mobility diameter.

2.4.3. Particle morphology, effective density and volatility

To allow conversion of the particle number size distributions measured by the SMPS into mass size distributions, information about particle effective density is required. Accordingly, the particle effective density is needed to determine the mass dose to the lung. This is crucial for porous agglomerated particles, such as fresh emissions from diesel exhaust for which the particle effective densities can vary considerably within the size range of emitted DEP (Rissler et al., submitted for publication; Park et al., 2003).

The effective density (ρ_{eff}) of a particle is defined as the particle mass (m_{agg}) per volume unit, assuming that the diameter of the particle is equal to the mobility diameter (d_{me}) measured by the DMA:

$$\rho_{eff} = m_{agg}/(\pi d_{me}^3/6). \tag{2}$$

Characterization of the particle effective density was performed using the DMA–Aerosol Particle Mass Analyzer (DMA–APM), further described in McMurry et al. (2002). In the DMA–APM system, the mass of individual particles is measured by the APM after being selected according to their mobility diameter by a DMA. In the set-up, a long column DMA (TSI, Shoreview, MN), operating at an aerosol flow rate of 0.8 l/min and a sheath flow rate of 6 l/min, and an APM model 3600 (Kanomax Japan), operating at an aerosol flow rate of 0.8 l/min, were used. Before being selected by the DMA, the particle passed through a (^{63}Ni) bipolar charger (or neutralizer) resulting in an equilibrium charge distribution. During the experiments, particles of d_{me} between 50 and 450 nm were characterized. A schematic diagram of the set-up is shown in Fig. 2. The measured effective densities were corrected using Poly Styrene Latex (PSL) density standards (Duke Scientific Corp., USA), as described in McMurry et al. (2002). A specially written APM program was used for DAQ, since the number concentrations were too low for the original DAQ program provided by the Kanomax.

For agglomerates formed in diffusion limited processes, the relation between m_{agg} and d_{me} has been shown in several previous studies (Park et al., 2003; Maricq & Xu, 2004; Olfert et al., 2007; Pagels et al., 2009; Malik et al., 2011a) to be well

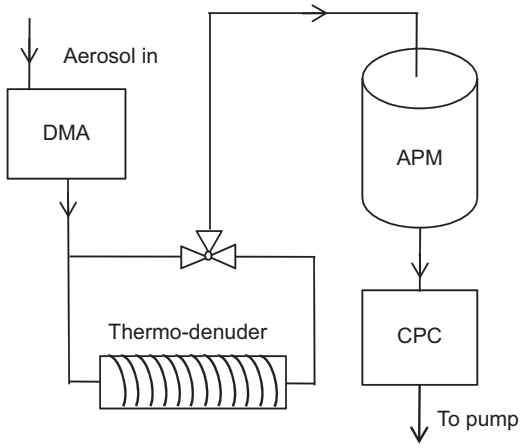

Fig. 2. Schematic diagram of the DMA–APM set-up. The set-up is used for measuring particle effective density of agglomerates and volatile mass fraction on-line. Particles with a single d_{me} are selected with the DMA and thereafter their mass is measured by the APM. A thermo-denuder is used to determine the volatile mass fraction.

described by a power law function according to

$$m_{agg} = K d_{me}^{\varepsilon_m} \quad (3)$$

where the exponent, ε_m, is referred to as the mass–mobility exponent. Here ε_m is used only to describe the mass–mobility relation over the size distribution and not as a fundamental fractal dimension (Sorensen, 2011). For distributions where m_{agg} can be well described by a power law function, so can the particle effective density.

By operating a thermo-denuder (TD) in series in between the DMA and the APM, and by scanning alternately through the TD and bypassing it, the mass fraction of volatile material for agglomerates of a given d_{me} was determined (Sakurai et al., 2003b; Malik et al., 2011b). The TD (stainless steel tube with inner diameter of 31 mm, about 300 mm long) was operated to 300 °C. More details about the set-up and data reduction techniques are given in Rissler et al. (submitted for publication).

Particles were collected during both operating modes on carbon coated copper grids with a diameter of 3 mm by using an electrostatic precipitator (NAS Model 3089, TSI Inc.) for subsequent analysis by High-Resolution Transmission Electron Microscopy (HR-TEM) (60 KeV PHILIPS CM10). Primary particle size (d_{pp}) was analyzed manually using the software "ImageJ" (Image Processing and Analysis in Java). For each type of running conditions, ~150 primary particles were sized from randomly selected aggregates.

2.4.4. Particle restructuring

One critical issue for the respiratory tract deposition measurements with polydisperse aerosols is whether the agglomerates restructure in the lungs when humidified and heated to 37 °C (Löndahl et al., 2006). If restructuring occurs between the inhalation and exhalation tank, the mobility diameter of a given particle is altered, which will lead to misinterpretation of the deposition pattern. To test the behavior of the soot agglomerates particles of one d_{me} (20–300 nm) at a time were selected in a DMA and thereafter heated to 45 °C or exposed to RH > 95%. The aerosol was then equilibrated at ambient temperature and dry conditions before the imposed change in d_{me} was quantified by an SMPS.

Upon humidification, the particles showed no sign of restructuring. This is consistent with observations by Pagels et al. (2009) who showed that soot coated with hydrophilic substances restructured at elevated RH at subsaturation, while fresh hydrophobic soot did not. Fresh diesel soot produced from diesel fuels of a higher sulphur content than in this study might be coated by a thin hygroscopic layer and thus restructure upon humidification. During the transient mode, no evaporation or restructuring occurred at 45 °C, whereas shrinkage of at most ~3% in diameter was observed for particles smaller than 50 nm during idling. This was not considered any major problem for the RESPI measurements.

2.5. Total deposited number, surface area and mass (volatile and non-volatile)

From the measured size-dependent deposition probability the total deposited fraction (TDF) of the whole particle size distribution was determined with respect to number (N), surface area (SA), and mass (m). The TDF strongly depends on the size-dependent deposition probabilities and the moment of the particle size distribution considered (N, SA or m). How surface area size distributions and mass size distributions are calculated from SMPS data is described later in this section, where a new method to estimate SA is suggested. From the TDF, the deposited dose (by number, surface area, or mass) to the lung is calculated as

$$Dose = TDF \cdot C_{in} \cdot t \cdot Q \quad (4)$$

where C_{in} is inhaled concentration by number, surface area or mass, t is exposure time and Q inhaled volume flow. Furthermore, the deposited dose was determined for a supposed mass concentration level of 1 μg/m^3 and an exposure time of 1 h, based on the deposition patterns, particle number size distributions and inhalation flow rates found in this study.

The mass size distributions and total mass concentrations were calculated from the measured SMPS number distributions using the particle effective densities from the DMA–APM. The mass size distributions, and mass doses, were separated into volatile and non-volatile mass fractions using the volatile fraction over size according to the DMA–TD–APM measurements.

In this study, a new model for estimation of the deposited surface area of the agglomerates (SA_{agg}) is proposed, applied and compared to the surface area estimated under the assumption that the particles are spherical. The model requires the following input:

(i) mass of the individual agglomerates as a function of mobility diameter $m_{agg}(d_{me})$,
(ii) primary particle size (d_{pp}), and
(iii) particle number size distribution ($dN_{agg}/d \log d_{me}$).

In this study, $m_{agg}(d_{me})$ was measured by the DMA–APM system, d_{pp} by TEM image analysis and $dN_{agg}/d \log d_{me}$ by the SMPS.

The number of primary particles composing the agglomerates (N_{pp}) was estimated from $m_{agg}(d_{me})$ and d_{pp}, assuming that the density of the primary particles (ρ_{pp}) was 1.8 g/cm^3 (Mullins & Williams, 1987; Dobbins, 2002; Park et al., 2004)

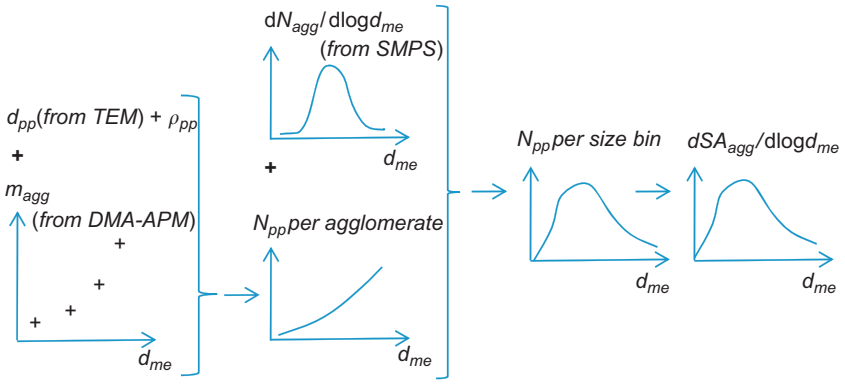

Fig. 3. Principle of the model proposed for estimating surface area distribution of the agglomerates. Denotations: d_{pp} primary particle size, m_{agg} the mass per aggregate, $dN_{agg}/d\log d_{me}$ agglomerateregate particle number size distribution, N_{pp} number of primary particles, $dSA_{agg}/d\log d_{me}$ surface area size distribution.

and that the point of contact between the primaries in the agglomerate was infinitesimal. The number of primary particles in an agglomerate of a given d_{me} is then given by (Bladh et al., 2011; Rissler et al., submitted for publication)

$$N_{pp}(d_{me}) = \left(\frac{m_{agg}(d_{me})}{m_{pp}}\right) = \left(\frac{m_{agg}(d_{me})}{\rho_{pp}\cdot(\pi d_{pp}^3/6)}\right) \tag{5}$$

where m_{pp} is the mass of one primary particle. Thereafter the total number of primary particles composing all aggregates of a specific d_{me} (N_{pp} in an agglomerate multiplied by N_{agg}) was calculated using measured $dN_{agg}/d\log d_{me}$. The principle of the model is shown in Fig. 3. Thus, the surface area of individual agglomerates is given by (combining Eqs. (3) and (5))

$$SA_{agg}(d_{me}) = N_{pp}(d_{me})SA_{pp} = m_{agg}(d_{me})/m_{pp}SA_{pp} = \frac{6Kd_{me}^{\varepsilon_m}}{\rho_{pp}d_{pp}}. \tag{6}$$

where SA_{pp} is the surface area of one primary particle. The last step is true only if the mass can be described by a power function. If so, SA is proportional to $d_{me}^{\varepsilon_m}$, while for spherical particles to d_{me}^2. Note that an error in d_{pp} results in an error in SA_{agg} proportional to $1/d_{pp}$. Inherent in the model is that, for aggregates where the mass–mobility relation can be described by a power law function, the surface area per mass unit is constant over size and determined solely by ρ_{pp} and d_{pp} (see Eqs. (3) and (6)).

The surface area model was also applied in the study of gold agglomerates by Messing et al. (in press).

3. Results and discussion

3.1. Aerosol properties

3.1.1. Mass concentration and chemical composition

The mass concentration of DEP in the chamber, measured by the TEOM, was (± 1 s.d.) 300 ± 2 μg/m^3 during transient engine running conditions and 59 ± 5 μg/m^3 during the idling conditions. Corresponding data from the filter measurements were 266 ± 32 μg/m^3 and 64 ± 14 μg/m^3, respectively. During transient engine running conditions the carbon analysis showed an OC/TC ratio of 11%, while a higher organic fraction of 43% was found during idling conditions.

3.1.2. Particle size distributions

The size distributions could be well described by lognormal functions (Hinds, 1999, Eq. (4.41)). The particle number size distribution generated in the chamber during the transient cycle was unimodal and consisted of an accumulation mode with a geometric mean mobility diameter (GMD) of ~88 nm, with a geometric standard deviation (σ_g) of 1.97. Two modes were found for the idling aerosol: a nucleation mode with a fitted GMD of ~16 nm and σ_g of 1.52, and an accumulation mode with a GMD of 75 nm and σ_g of 1.98. The modal ratio with respect to number was ~0.5. All fitted $GMDs$ and σ_g are presented in Table 2 and the particle number size distributions are shown in Fig. 4. For both aerosols, the accumulation mode was stable in concentration and size, while the nucleation mode, present during idling, showed a higher variability. The total number concentration during the transient cycle was on average ~222,000 cm^{-3} (relative s.d. 6%) and during idling ~82,000 cm^{-3} (relative s.d. 27%); and if normalized to number concentration per 1 μg, it was 1560×10^6 and 2250×10^6 particles, respectively.

Our results are consistent with several previous studies showing that the particles in diesel exhaust emissions generally are dominated by an accumulation mode composed of agglomerated soot particles formed at higher temperatures during incomplete combustion in the engine. At lower exhaust temperatures, volatile compounds (mostly organics) either

Table 2
Number size distributions were measured using the SMPS and mass size distributions derived from SMPS and DMA–APM data. Surface area distributions were modeled (see Section 2.5). Values in parentheses are only shown for comparison and are based on assuming spherical particles. For surface area and mass size distributions, the nucleation mode particles were insignificant. During idling, the number fraction of the nucleation mode was 0.49. For SAagg values in paranthesis.

			Transient	Idling
Number distribution	Nucl mode	*GMD* (nm)	–	16
		σ_g	–	1.52
	Acc. mode	*GMD* (nm)	88	75
		σ_g	1.97	1.98
Number per 1 μg			$1560 \cdot 10^6$	$2250 \cdot 10^6$
Surface area distribution		*GMD* (nm)	219 (192)	230 (170)
		σ_g	1.81	1.87
SA_{agg} per 1 g (m^2)			152 (78)	86 (51)
Mass distribution		*GMD* (nm)	219 (274)	230 (288)
		σ_g	1.81	2.00
Volatile mass per 1 μg (μg)			0.06	0.23

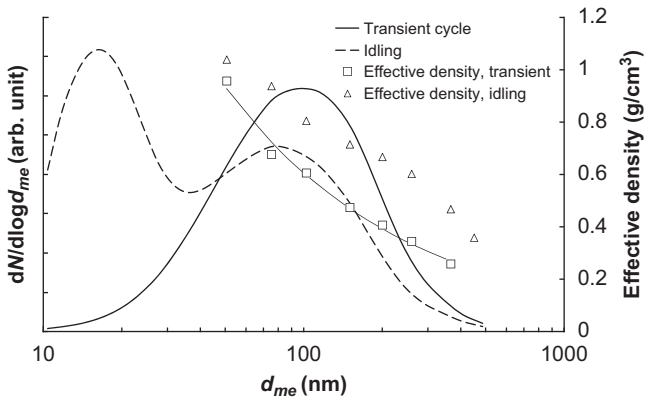

Fig. 4. Number size distributions during idling and transient driving cycles. Relative number concentration of the two aerosols are normalized to 1 μg/m^3 (left axis). In the graph, the effective density measured by the DMA–APM system is shown (right axis). The power law function, fitted to transient data, is also shown.

nucleate to form a nucleation mode of volatile particles or condense onto the soot agglomerated to yield a coating of organic compounds (Sakurai et al., 2003a,b; Maricq, 2007). The formation of a nucleation mode is very sensitive to engine operating and exhaust dilution conditions (Maricq, 2007). This is typically valid for heavy duty diesel engines with no diesel particulate filters and fuel with low sulphur content.

The mass size distribution spectra were based on measured number size distribution and DMA–APM data, and the surface area distribution estimated according to the model presented in this paper. Fitted distribution parameters are presented in Table 2. For comparison, the corresponding parameters assuming spherical particles are presented. The shift in *GMD* going from number to surface area or mass is determined by the exponential used for d_{me} (d^2 for spheres when estimating surface area distributions and d^3 when estimating mass [Hinds, 1999, Eq. (4.49)]). For agglomerates for which the mass–mobility relation can be described by a power law function (Eq. 3), both mass and surface area are proportional to $d^{\varepsilon m}$ (Eq. 6) resulting in identical *GMD*s for both surface area and mass size distributions, according to our model.

The surface area was determined to 152 m^2/g during transient and 86 m^2/g during idling, estimated by the semi-empirical model here suggested. The data is presented in Table 2. Surface area values assuming spherical particles are also presented. These values are normalized to the same mass as SA_{agg}. Normalizing with the mass estimated from the SMPS data, assuming spherical particles, results in even lower surface area concentrations.

Another frequently used surface area metric is BET (Brunauer, Emmett, and Teller). For heavy-duty engine emissions, NIST (US National Institute of Standards and Technology) reports a particle surface area of 108 m^2/g (NIST 1650b, 2006), for samples outgassed in vacuum at 120 °C, which is similar to that reported here. The disadvantages with the BET method are that the method is offline, requires a large sample (> 10 mg), volatile material might be lost, and it gives no size-resolved information. There are also arguments that the BET method underestimates surface area due to agglomeration on the filter (Giechaskiel et al., 2009).

The "active" surface area can also be determined using a diffusion charger (DC). One advantage with this method is that the DC is a relatively cheap instrument with high time resolution, and that the measurement does not require any off-line

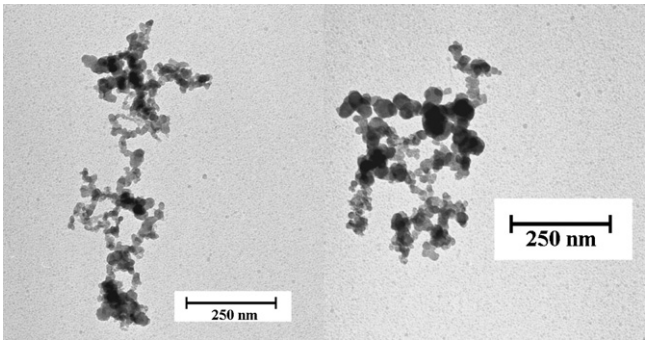

Fig. 5. TEM image of a typical agglomerate. The particle was collected during transient running conditions.

info from for example TEM (Ntziachristos et al. Giechaskiel et al., 2009). The disadvantage with the DC method is that the active surface area does not have physically correct size dependence for a surface area measurement even for spheres (for DC method typically proportional to $d_{me}^{1.4}$ at 100–200 nm) and relies on careful calibration in the relevant particle size range. Another commonly used online monitor is the NSAM (Asbach et al., 2009) which measures the lung deposited surface area particle concentration. This has been shown up to about 300 nm for spheres but remains to be shown for agglomerates.

3.1.3. Particle morphology and volatility

TEM images revealed agglomerated particles (Fig. 5). The DMA–APM measurements also showed that both types of DEP had decreasing effective densities with increasing d_{me} (Fig. 4), which is typical for agglomerated particles. These ranged from $\sim$1 g/cm^3 for the smallest particles measured (d_{me} 50 nm) down to 0.26 and 0.47 g/cm^3 for particles of 366 nm for transient cycle and idling, respectively.

For particles generated during the transient cycle, the mass–mobility relation over size could be well described by one exponent, determined to 2.35 (K=9.21, if the units are in meter [m] and gram [g]. K is given in Eq. (3)). This is similar to observations made previously in studies employing diesel exhaust, as well as for flame soot generators (Park et al., 2003; Maricq & Xu, 2004; Olfert et al., 2007; Malik et al., 2011a). The mass–mobility exponents reported by Park et al. (2003) for a John Deere engine, at 10–75% load, measured using the DMA–APM technique were 2.33–2.41 with effective densities ranging from 1.20 g/cm^3 for 50 nm particles down to 0.30 for 300 nm particles.

The volatility measurements showed that during the transient cycle, on average, $\sim$6% of the mass of the agglomerates was volatile at 300 °C. The volatile fraction was relatively constant over the whole size range covered (ranging from 5–8%) with no trend of increasing or decreasing volatility over size. This result, together with the dominating EC fraction determined by the filter measurements (as given in Section 3.1.1.), strongly supports the suggestion that the DEP during the transient engine conditions were composed of a typical soot dominated mode of agglomerates.

During idling, the exhaust particles covered by the DMA–APM measurements could not be well described by one mass–mobility exponent. This is presumably explained by a higher amount of organics found during idling conditions, indicating that the particles were not pure soot agglomerates, which was confirmed by the OC/EC analysis. When heated to 300 °C, the volatile mass fraction of the DEP formed during idling engine conditions was strongly size-dependent, ranging from 38% for the 50 nm particles to 12% for the 450 nm particles. 50 nm is the lower mass limit of the DMA–APM used for soot particles. The DMA–APM measurements do not cover the nucleation mode. At 50 nm only 3% of the size distribution belongs to the nucleation mode.

Also during idling, the accumulation mode showed decreasing effective densities over size, indicating that the particles were agglomerates, in line with the results from transient engine conditions. However, compared to particles formed during the transient running conditions, the accumulation mode had higher effective densities and contained more volatile matter. This is caused by a higher concentration of emitted volatile compounds during idling compared to the transient cycle, which results in both nucleation and a higher degree of condensed volatile material onto the accumulation mode particles (Sakurai et al., 2003a).

Coagulation of nucleation mode particles onto the soot structures and concentration dependent partitioning in the mixing/exposure chamber (i.e. after the second dilution step) cannot be excluded. However, APM measurements performed during idling engine conditions at both 50 μg/m^3 and 300 μg/m^3 showed no significant difference in the amount of volatile matter as a function of size, indicating that such effects are small. More details about the DMA–APM data set are found in Rissler et al. (submitted for publication).

These observations are in full agreement with the general consensus of DEP characteristics: that the fine particle fraction consists of an accumulation mode, composed of fractal-like soot agglomerates with more or less condensed organic material on the surface (Kittelson, 1998; Maricq, 2007), and to a varying degree nucleation mode particles, composed of volatile organics and/or sulphuric acid (from the fuel or lubricant oils). TEM images confirmed that the

accumulation mode particles mainly consisted of agglomerated soot particles. The primary particle size was determined to 22 nm (± 7 nm) for the transient driving cycle and 28 nm (± 11 nm) during idling.

3.2. Respiratory tract deposition

3.2.1. Size-dependent deposited fraction and parameterization

The particle deposition patterns ($DF(d)$) in the human respiratory tract of two different types of DEP were measured in 9 healthy subjects during spontaneous breathing. The resulting average deposition pattern is shown in Figs. 6 and 7, also showing the standard deviation (s.d.). Individual deposition patterns for each subject are found in the supplemental information in the appendix.

Each individual subject had similar deposition patterns for both types of DEP. For each type of DEP two deposition measurements were performed on the subjects. The mean difference in $DF(d_{me})$ for each subject of the two measurements of the same type of DEP was ± 0.03, averaged over the size interval measured, which was the same difference found for

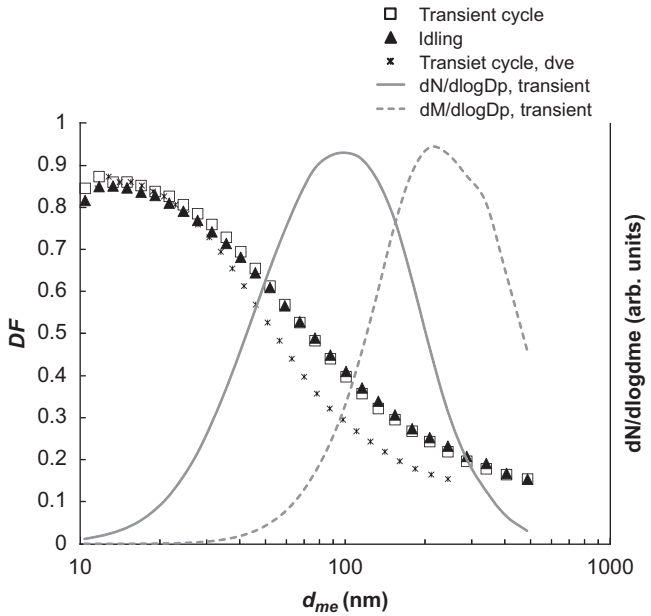

Fig. 6. Averaged lung deposition pattern for each DEP type. The particle number and mass size distributions for the transient driving cycle are also shown in the graph. The deposition probability as a function of volume equivalent diameter is also given—note that the x-axis for this curve is d_{ve}.

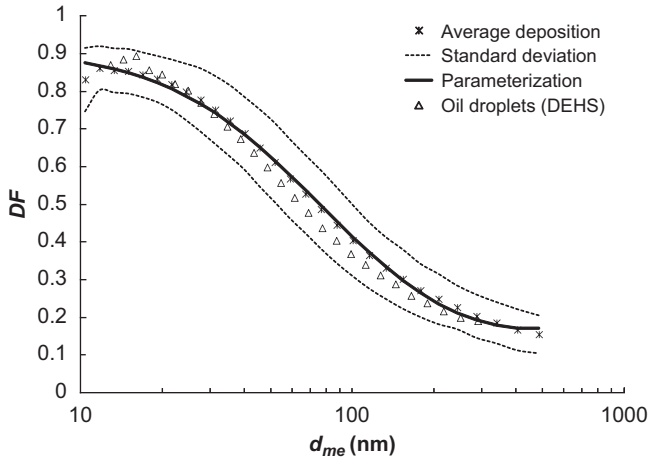

Fig. 7. Total average deposition pattern ± 1 s.d. illustrating the inter-subject variability. For comparison, the deposition pattern found for spherical oil droplets (DEHS) from Löndahl et al. (2007) is plotted.

each subject between the two DEP types. The inter-subject variability was larger with a standard deviation of 0.08, averaged over the size interval measured. The largest observed inter-subject difference in $DF(d_{me})$ was 0.33 (occurring $\sim$70 nm for both DEP exposures).

The average lung deposition pattern was parameterized by fitting a four parameter function to the data:

$$DF(d_{me}) = a_k + b_k d_{me} - \frac{1}{c_k (C_c/d_{me})^{d_k} + 1} \tag{7}$$

where a_k, b_k, c_k and d_k are the fitted parameters and C_c the Cunningham correction term. The parameters are a_k: 0.924, b_k: 0.25, c_k: 0.0658, and d_k: 0.76. For illustration, the resulting measured deposition pattern after converting d_{me} to volume equivalent diameter is shown in Fig. 6.

3.2.2. Effect of agglomeration state on deposited fraction

From the particle characterization using the DMA–APM system, it was shown that the particles produced during the transient cycle were highly agglomerated and could be described by one mass–mobility exponent, while those produced during idling had higher effective densities and could not be described by a power law function (Fig. 3). This difference in particle agglomeration state between the two types of DEP did not appear to affect the lung deposition pattern for particles of the same mobility diameter, shown in Fig. 6.

This was further confirmed when comparing the deposition patterns found in this study with those found in a previous study of spherical oil droplets (Löndahl et al., 2007), shown in Fig. 7. In Löndahl et al. (2007), tidal volumes and breathing frequencies, ± 1 s.d., were 0.72 ± 0.15 L and 12.4 ± 2.3 min^{-1} respectively (compare with Table 1).

The dominating deposition mechanism in the respiratory tract of particles below 500 nm is diffusion. Deposition by diffusion is governed by the particle diffusivity (D), which can be related to mechanical mobility (B) and mobility equivalent diameter through Stokes–Einstein equation and Stoke's Law:

$$D = kBT = \frac{3kT\eta d_{me}}{C_c(d_{me})} \tag{8}$$

where k is the Boltzmann constant, η is kinematic viscosity of air, C_c is the Cunningham correction term and T is temperature. This means that d_{me} can be written as a function of diffusivity, which implies that particle size as d_{me} is the relevant equivalent diameter describing deposition of particles in the respiratory tract—when diffusion is the dominating deposition mechanism. Thus, in the diffusion-dominated regime, the deposition fraction as a function of d_{me} is independent of shape and density, as confirmed by the present results.

An increased deposition due to interception could occur because of the large physical size of the agglomerate, as shown by Scheckman & McMurry (2011). Their study used a silicone rubber lung cast prepared from the airways from a 64-year old lung donor, while in our study the lungs of 9 healthy volunteers were used. The cast used by Scheckman & McMurry (2011) simulated only lung generation 3–9. With a simulated inspiratory flow rate of 8 l/min (compared to 9 in this study) using agglomerates with $\varepsilon_m = 2.4$ and $d_{pp} = 35$ nm, they found a slight increase in the deposition fraction from about 0.03 to 0.04 in the cast. The majority of 50–500 nm particles that deposit in the respiratory tract, deposit in the pulmonary region, which means that our results on DF are dominated by the pulmonary region. Thus, our and Scheckman and McMurry's results may not be in disagreement.

One issue when characterizing agglomerates using the SMPS is the possible alignment of the agglomerates (Zelenyuk & Imre, 2007) in the electrical field of the DMA (the size selection part in the SMPS). This would result in an underestimation of d_{me} and requires further investigation for DEP.

3.2.3. Total deposited fraction

The total deposited fractions of the two particle size distributions were determined for each test subject from $DF(d_{me})$ (Table A2). The average TDFs for number, surface area and mass are presented in Table 3a. Surface area was calculated using both the model for agglomerates presented here (agglomerates with point contact between the primary particles), and assuming spherical particles. The total deposited number fraction (± 1 s.d.) for particles formed under transient running conditions was 0.47 ± 0.10 and for idling 0.65 ± 0.07. The difference in TDF between the two types of DEP is explained by the shift in size distribution towards larger sizes for the transient cycle, thereby peaking closer to the minimum in the $DF(d_{me})$ curve than particles formed during idling.

In comparison to Morawska et al. (2005), the deposition fraction found in the present study was higher for small particles (< 150 nm) and lower for large particles (150–500 nm). By particle number, the total deposition fraction reported here is higher than that reported in Morawska et al. (2005) (0.30). However, TDF is strongly dependent on particles size distribution and part of the difference is explained by differences in particle number size distributions. Furthermore, there were several differences in the studies, such as nose/mouth breathing, subject breathing frequency (significantly higher in Morawska et al., 2005), and last but not the least in sampling systems.

The differences were minor between the two engine running conditions when comparing the total deposited fraction for surface area or mass. The reason is that the nucleation mode plays a less important role for the deposited SA and m than for number. The TDF during transient and idling engine conditions was, for SA_{agg} 0.27 and 0.30, respectively, and for mass

Table 3
The total deposited fraction and dose to the lungs. (a) The total deposited fraction with respect to number, surface area, and mass of particles generated during idling and transient cycles. The deposited fraction of the volatile mass (at 300 °C) is also given. (b) The lung deposited number (N), surface area (SA) and mass (m) per 1 $\mu g/m^3$ and during 1 h exposure. Surface area is calculated using two approximations: spherical particles (sph) or agglomerates (agg) of primaries joint with point contact.

(a) Total deposited fraction (TDF)

	TDF_N	TDF_{SAsph}	TDF_{SAagg}	TDF_m	$TDF_{volatile,\ m}$
Transient	0.47 ± 0.10	*0.29 ± 0.08*	0.27 ± 0.07	0.27 ± 0.07	0.27 ± 0.07
Idling	0.65 ± 0.07	*0.32 ± 0.07*	0.30 ± 0.06	0.28 ± 0.06	0.32 ± 0.07

(b) Deposited dose per 1 μg/m³ and hour

	N ($\cdot 10^6$)	SA_{sph} (mm^2)	SA_{agg} (mm^2)	Mass (μg)	Volatile mass (μg)
Transient	363 ± 104	*11.4 ± 3.8*	20.1 ± 7.1	0.134 ± 0.048	0.0083 ± 0.0029
Idling	728 ± 155	8.3 ± 2.5	12.9 ± 3.8	0.140 ± 0.044	0.036 ± 0.011

0.27 and 0.28, respectively. All results given in Table 3 are based on the measured deposition patterns, along with the particle size distributions presented in Table 2.

Determination of particle mass size distributions and the total mass deposition fraction (TDF_m), or dose, from number size distributions measured with a DMA (classifying particles according to d_{me}) is always based on an assumption of particle effective density. For agglomerated particles, which typically have strongly decreasing effective density with particle size, the assumption that the particle effective density is constant over size will lead to a mass size distribution shifted towards larger sizes, and higher absolute mass concentrations, than when fully accounting for agglomerated particles. Assuming spherical particles would result in an underestimation of the total deposition fraction by mass, TDF_m, of ~10%. This relatively small effect of effective density can be explained by the size distribution that, in this study, peaks at the minimum in the deposition fraction curve (Fig. 6) making the TDF_m less sensitive to a shift in size.

3.2.4. Total deposited dose (by number, surface area and mass)

The deposited dose (± 1 s.d.) (i.e. the total amount of particles deposited) are presented in Table 3b for both aerosols. The dose was normalized to a mass concentration level of 1 $\mu g/m^3$ and one hour of exposure.

The largest observed difference between idling and transient driving conditions was the dose by particle number, with a two times higher dose during idling than during transient driving conditions. As for TDF_N, this was due to the nucleation mode being present in the exhaust from the idling engine, for which the deposition probability is high (Fig. 4). In general, persons with a high TDF also received a high total dose, with some exception due to the inhaled volume.

For the transient cycle aerosol, the surface area dose was determined to 20.1 mm^2 (± 7.1) (per $\mu g/m^3$ and hour) and for the idling aerosol 12.9 mm^2 (± 3.8). Values in parenthesis are 1 s.d. The mass dose was very similar for both driving conditions (0.14 μg [± 0.04] during transient cycle compared to 0.13 μg [± 0.05] during idling). The mass was dominated by soot. However, during idling a considerable fraction was volatile (at 300 °C), 26%, whilst during the transient cycle only 6% (using the DMA–TD–APM method). The volatile mass dose is given in Table 3b. In this study, most of the compounds volatile at 300 °C are likely to be organic. Separating the effects of organics and non-soluble particulates in such a manner was suggested and discussed in Giechaskiel et al. (2009). Note that the total deposited number of particles was higher during idling than during the transient cycle, while the modeled deposited surface area was 36% lower during idling.

The absolute surface area dose is much more sensitive to the agglomeration state than the TDF_{SA} (see Table 3). Two values for the deposited surface area are given in Table 3. These were calculated using two different assumptions: (*i*) that the particles were spherical (SA_{sph}) or, (*ii*) that the particles were agglomerates composed of equally-sized primary particles joined together at an infinitively small area (SA_{agg}). Since TEM images and DMA–APM measurements clearly show that the particles were of an agglomerate structure, the assumption of spherical particles is obviously erroneous and would lead to an underestimation of the total deposited surface area by 36–43% (highest value referring to transient running conditions). However, TEM images also show a considerable necking between the primaries. Assuming that the contact areas between the primary particles are infinitively small will lead to an overestimation of the deposited surface area. The true surface area probably lies in between the two extremes: SA_{sph} and SA_{agg}. For particles emitted during transient driving, the latter approximation is probably closer to reality, while the particles formed during idling were more compact due to the higher degree of coating with volatile material. If the agglomerates break up into primary particles when deposited in the lung fluid (Rothenbacher et al., 2008), the agglomerate assumption would be close to the true surface area. As a next step for improving the surface area model, necking between primary particles will be considered.

Lall et al. (2008) have previously suggested that the surface area could be estimated from information on the individual primary particles composing the agglomerates, and their model was applied for lung deposition predictions by Wang & Friedlander (2007). In that model, the estimate of the number of primaries in each agglomerate particle was determined from measured mobility distributions, assuming that the drag force on the agglomerates was determined by the sum of the drag forces on each primary particle in the agglomerate, neglecting the shielding effect by neighboring primary

particles. Neglecting the effect of shielding will likely lead to an underestimation of N_{pp}, especially for larger agglomerates. In Lall et al. (2008) the same assumption of infinitesimal point of contact between the primaries is used. Applying the model using N_{pp} from DMA–APM data should improve the accuracy of the deposited surface area.

The mass dose is very sensitive to the particle effective density when estimated from SMPS number size distributions. Assuming that the particles were spherical and composed of pure soot (density of $\sim 2\ g/cm^3$) would result in overestimating the dose by 70–170%. In this study the particle effective densities were measured, and no assumption regarding density was needed.

3.2.5. Inter-subject variability

There was considerable variability in TDF and deposited dose between the individual subjects. The highest dose a subject received was twice as high as that of the subject with the lowest dose, with respect to number ($\sim$103% higher during idling and 107% during transient). For surface area and mass, the difference was even larger. The corresponding numbers were 140% for idling and 144% for transient (average for both DEP types). The large inter-subject variability that was found in the study strengthens the idea that some people are more susceptible to ambient ultrafine particles than others (Chalupa et al., 2004; Löndahl et al., 2007).

Associations were found between total deposited number fraction, tidal volume, and breathing frequency for the idling aerosol, showing an increasing TDF_N with increasing V_T ($r=0.840$, $p<0.01$) and a decreasing TDF_N with increasing f ($r=-0.774$, $p<0.05$). Even though no significant associations between TDF and breathing patterns were found for the transient driving cycle, the trends were the same as during idling. Similar relationships between total deposition and tidal volume, and deposition and breathing frequency have been found in previous studies (Jaques & Kim, 2000; Kim & Jaques, 2005; Heyder et al., 1975; Brand et al., 2000; Tu & Knutson, 1984). In this study, no significant correlations between lung function and TDF were found.

A significant positive association was found between forced vital capacity (FVC) and deposited dose by number ($r=0.806$, significant at the 0.01 level) for the idling aerosol. For the idling aerosol, the deposited number of particles also correlated with minute volume (MV) ($r=0.891$, $p<0.01$) and FEV1 ($r=0.73$, $p<0.05$). The deposited number of particles during both idling and the transient running cycle correlated with V_T (for idling $r=0.739$, $p<0.05$, for transient $r=0.725$, $p<0.05$).

For surface dose, associations were found with V_T ($r=0.697$, $p<0.05$) and MV ($r=0.672$, $p<0.05$) during idling engine conditions and with V_T ($r=0.669$, $p<0.05$) for transient running conditions. For the idling aerosol, the deposited mass dose also correlated with V_T ($r=0.685$, $p<0.05$). In some earlier studies, inter-subject variability has been deduced to differences in lung morphology (Heyder et al., 1982).

There was a significant difference between the idling and transient cycle for TDF_N ($p<0.001$), for absolute surface area dose ($p<0.05$), and mass dose ($p<0.0001$). For the individual test subjects, the TDF_N during idling and transient running cycle correlated well with $r=0.906$ ($p<0.01$). That is to say that a subject with a high deposition during idling also had a high deposition during the transient cycle. The deposition patterns of all individuals are presented in the appendix, Table A1.

3.2.6. Implications for health effects

Experimental human exposure-studies have been performed in the same exposure chamber employing diesel exhaust generated during both idling and the transient driving conditions and were evaluated with respect to cardiovascular and respiratory endpoints. For both driving conditions, similar effects on vasomotor function and endogenous fibrinolysis have been shown in a number of studies (Mills et al., 2005; Törnqvist et al., 2007; Barath et al., 2010; Lucking et al., 2011). When it comes to respiratory effects of diesel exhaust generated during idling and transient driving, so far only one study has been performed using the transient driving condition. It showed that the airway inflammatory response may be less pronounced compared with after idling (Salvi et al., 1999; Sehlstedt et al., 2010). It is plausible that differences in particle deposition and the characteristics investigated in this study (size, morphology, volatile vs. core mass fraction, etc.) may be one among several possible explanations behind similarities and differences in cardio-respiratory responses. The deposited dose by number was higher during idling than during the transient running condition, as was the volatile organic fraction (containing a small fraction PAHs). The deposited surface area was, on the contrary, lower during idling while mass doses were similar. However, in the human exposure studies for idling engine, two different engines have been used and therefore this will need further evaluation.

4. Summary and conclusion

Diesel emissions constitute a large part of the vehicle-generated ambient aerosol in cities. To be able to understand what role diesel particulate emissions play, it is important to predict the actual dose of diesel particles deposited in the human respiratory tract with respect to number, surface area and mass.

In this study, human respiratory tract deposition fractions over the size interval of 10–500 nm were determined for two types of diesel exhaust particles: those formed during idling and transient engine running conditions. The mass dose was estimated by combining the deposition fraction pattern with the number size distribution and the mass of the individual agglomerates, measured by a DMA–APM set-up. A model for estimating surface area of the deposited agglomerates was suggested and applied. Furthermore, the mass dose was separated into the physical dose and the chemical dose (Table 3) using volatile mass fractions of the particles at 300 °C (Giechaskiel et al., 2009).

A large inter-subject variability was observed with some subjects receiving a dose that was twice as high as the dose of others when exposed to the same particle concentration. The large inter-subject variability found in the study strengthens

the hypothesis that some people are more susceptible to ambient ultrafine particles than others (Chalupa et al., 2004; Löndahl et al., 2007). Associations were found between total deposited fractions, tidal volume and breathing frequency, showing increasing TDF with increasing tidal volume and decreasing TDF with increasing breathing frequency.

The measured size-dependent deposition fraction of the two types of agglomerated exhaust particles was nearly identical (Fig. 6) and closely resembles that of spherical hydrophobic particles (Löndahl et al., 2007). Thus, there is no measurable effect of particles agglomeration state on the particle size-dependent deposition fraction, if described as a function of mobility diameter. The explanation for this is that the dominating deposition mechanism of particles below ~500 nm is diffusion, and that the diffusivity is a function of mobility diameter, independent of particle effective density. This is the type of diameter measured here and in most other studies in this size regime. The mobility diameter is, for spherical particles, identical to the volume equivalent diameter (geometric diameter). As a comparison, the resulting deposition curve is plotted in Fig. 6 as a function of volume equivalent diameter (converted using the DMA–APM results).

Whilst the deposition probabilities over size were very similar for the two aerosols, there was a difference in the observed total deposited fraction and dose. The deposited number of particles was much higher for idling conditions (38% higher total deposited fraction and 101% higher dose per $\mu g/m^3$) than during transient driving conditions. The reason for the high deposition during idling is the presence of a nucleation mode (*GMD*: 16 nm), for which the probability of deposition is high. The nucleation mode is typically observed in ambient studies of diesel exhaust causing the dose to be higher than expected if only the soot mode is present.

The surface area and mass dose derived from number size distributions measured using DMAs techniques is very sensitive to assuming the correct particle morphology and particle effective density. Deriving the mass dose from measured deposition patterns and number size distributions, assuming that the particles were spherical, using a density of 2 g/cm^3 (soot), would result in overestimating the dose by 70–170%, compared to when using the effective densities measured by the DMA–APM. Deriving the deposited surface area assuming spherical particles resulted in a ~36–43% lower dose than when using the proposed model. The largest given differences, for both mass and surface area, are associated with the particles generated during the transient driving cycle, which had the lowest effective densities. The TDF with respect to mass and surface area was slightly larger during idling, but particles generated during the two driving conditions did not differ to any large extent (Table 3a). This is because the accumulation mode, present in both cases, accounted for the dominating part of surface area and mass. The surface area per $\mu g/m^3$ was lower during idling than during the transient cycle.

One advantage of using the model here suggested for surface area is that it is based on measured particle properties. Furthermore, most characterization is performed on-line and while airborne and this results in both time and size-resolved information. The size-resolved information may be important if deposition probability is size-dependent, as in the respiratory tract. The time and size resolution is also important for estimating mass dose.

Taken together, the deposition probabilities predicted by common dose models, such as the ICRP or the MPPD, for hydrophobic spherical particles applies well to diesel exhaust particles for mobility diameters as when measured using any DMA-based technique (SMPS, FMPS, EEPS, DMS, TDMA, etc.). However, the assumption of spherical particles leads to a substantial error when calculating the deposited surface area and particle mass. For this calculation it is necessary to consider particle agglomeration and effective density as outlined in this study. The present methodology makes it possible to better predict the actual dose of diesel particles deposited in the human respiratory tract with respect to number, surface area and mass. As diesel emissions constitute a large part of the combustion-generated ambient particulate matter air pollution, it is of major importance to improve the estimation of particle lung deposition and its association to negative health effects.

Acknowledgments

The following organizations are gratefully acknowledged: The Swedish Research Council for Environment, Agricultural Sciences and Spatial Planning (FORMAS) through projects 216-2009-1294, 216-2007-1223, and 2008-1467, the Swedish Governmental Agency for Innovation Systems (VINNOVA) through project 2009-01117, the Swedish Emission Research Program (EMFO) under contract AL 90 A 2006:10535, and the METALUND Swedish Council for Working Life and Social Research (FAS) Center.

Appendix A. Supporting information

Supplementary data associated with this article can be found in the online version at doi:10.1016/j.jaerosci.2012.01.005.

References

Asbach, C., Fissan, H., Stahlmecke, B., Kuhlbusch, T.A.J., & Pui, D.Y.H. (2009). Conceptual limitations and extensions of lung-deposited Nanoparticle Surface Area Monitor (NSAM). *Journal of Nanoparticle Research*, *11*, 101–109.

Alföldy, B., Giechaskiel, B., Hofmann, W., & Drossinos, Y. (2009). Size-distribution dependent lung deposition of diesel exhaust particles. *Journal of Aerosol Science*, *40*, 652–663.

Barath, S., Mills, N., Lundbäck, M., Törnqvist, H., Lucking, A., Langrish, J., Söderberg, S., Boman, C., Westerholm, R., Löndahl, J., Donaldson, K., Mudway, I., Sandström, T., Newby, D., & Blomberg, A. (2010). Impaired vascular endothelial function after exposure to diesel exhaust generated at urban conditions. *Particle and Fibre Toxicology*, *7*, 19.

Bladh, H., Johnsson, J., Rissler, J., Adulhamid, H., Olofsson, N.-E., Sanati, M., Pagels, J., & Bengtsson, P.-E. (2011). Influence of soot particle aggregation on time-resolved laser-induced incandescence signals. *Applied Physics B*10.1007/s00340-011-4470-y.

Brand, P., Friemel, I., Meyer, T., Schulz, H., Heyder, J., & Häussinger, K. (2000). Total deposition of therapeutic particles during spontaneous and controlled inhalations. *Journal of Pharmaceutical Science*, *89*, 724–731.

Broday, D., & Rosenzweig, R. (2011). Deposition of fractal-like soot aggregates in the human respiratory tract. *Journal of Aerosol Science*, *42*, 372–386.

Chalupa, D.C., Morrow, P.E., Oberdörster, G., Utell, M.J., & Frampton, M.W. (2004). Ultrafine particle deposition in subjects with asthma. *Environ health perspective*, *112*, 879–882.

Dobbins, R.A. (2002). Soot inception temperature and the carbonization rate of precursor particles. *Combustion and Flame*, *130*, 204–214.

Gebhart, J., Schiller-Scotland, Ch.F., Egan, M.J., & Nixon, W. (1989). On the relationship between experimental data for total deposition and model calculations—Part I: effect of instrumental dead space. *Journal of Aerosol Science*, *20*, 141–147.

Giechaskiel, B., Alföldy, B., & Drossinos, Y. (2009). A metric for health effects studies of diesel exhaust particles. *Journal of Aerosol Science*, *40*, 639–651.

Hart, J.E., Laden, F., Eisen, E.A., Smith, T.J., & Garshick, E. (2009). Chronic obstructive pulmonary disease mortality in railroad workers. *Occupational and Environmental Medicine*, *66*, 221–226.

Heyder, J., Armbruster, L., Gebhart, J., Grein, E., & Stahlhofen, W. (1975). Total deposition of aerosol particles in the human respiratory tract for nose and mouth breathing. *Journal of Aerosol Science*, *6*, 311–328.

Heyder, J., Gebhart, J., Stahlhofen, W., & Stuck, B. (1982). Biological variability of particle deposition in the human respiratory tract during controlled and spontaneous mouth-breathing. *Annals of Occupational Hygiene*, *26*, 137–147.

Hinds, W.C. (1999). *Aerosol Technology: Properties, Behaviuor, and Measurement of Airborne Particles* (2nd ed.). Wiley: New York.

Hofmann, W. (2011). Modelling inhaled particle deposition in the human lung—a review. *Journal of Aerosol Science*, *42*, 693–724.

Jaques, P.A., & Kim, C.S. (2000). Measurement of total lung deposition of inhaled ultrafine particles in healthy men and women. *Inhalation Toxicology*, *12*, 715–731.

Kim, C.S., & Jaques, P.A. (2005). Total lung deposition of ultrafine particles in elderly subjects during controlled breathing. *Inhalation Toxicology*, *17*, 387–399.

Kittelson, D.B. (1998). Engines and nanoparticles: a review. *Journal of Aerosol Science*, *29*, 575–588.

Lall, A.A., Rong, W., Mädler, L., & Friedlander, S.K. (2008). Nanoparticle aggregate volume determination by electrical mobility analysis: test of idealized aggregate theory using particle mass analyzer measurements. *Journal of Aerosol Science*, *39*, 403–417.

Löndahl, J., Pagels, J., Swietlicki, E., Zhou, J., Ketzel, M., Massling, A., & Bohgard, M. (2006). A set-up for field studies of respiratory tract deposition of fine and ultrafine particles in humans. *Journal of Aerosol Science*, *37*, 1152–1163.

Löndahl, J., Massling, A., Pagels, J., Swietlicki, E., Vaclavik, E., & Loft, S. (2007). Size-resolved respiratory-tract deposition of fine and ultrafine hydrophobic and hygroscopic aerosol particles during rest and exercise. *Inhalation Toxicology*, *19*, 109–116.

Löndahl, J., Pagels, J., Boman, C., Swietlicki, E., Massling, A., Rissler, J., Blomberg, A., Bohgard, M., & Sandström, T. (2008). Deposition of biomass combustion aerosol particles in the human respiratory tract. *Inhalation Toxicology*, *20*, 923–933.

Löndahl, J., Massling, A., Swietlicki, E., Brauner, E.V., Ketzel, M., Pagels, J., & Loft, S. (2009). Experimentally determined human respiratory tract deposition of airborne particles at a busy street. *Environmental Science & Technology*, *43*, 4659–4664.

Lopez, A.D., Mathers, C.D., Ezzati, M., Jamison, D.T., & Murray, C.J.L. (2006). Global and regional burden of disease and risk factors, 2001: systematic analysis of population health data. *Lancet*, *367*, 1747–1757.

Lucking, A.J., Lundbäck, M., Barath, S.L., Mills, N.L., Sidhu, M.K., Langrish, J.P., Boon, N.A., Pourazar, J., Badimon, J.J., Gerlofs-Nijland, M.E., Cassee, F.R., Boman, C., Donaldson, K., Sandström, T., Newby, D.E., & Blomberg, A. (2011). Particle traps prevent adverse vascular and prothrombotic effects of diesel engine exhaust inhalation in men. *Circulation*, *123*, 1721–1728.

Malik, A., Abdulhamid, H., Pagels, J., Rissler, J., Lindskog, M., Bjorklund, R., Jozsa, P., Visser, J., Spetz, A., & Sanati, M. (2011a). A potential soot mass determination method from resistivity measurement of thermophoretically deposited soot. *Aerosol Science and Technology*, *45*, 284–294.

Malik, A., Nilsson, P.T., Pagels, J., Lindskog, M., Rissler, J., Gudmundsson, A., Bohgard, M., & Sanati, M. (2011b). Methodology for sampling and characterizing internally mixed soot-tar particles suspended in the product gas from biomass gasification processes. *Energy and Fuels*, *25*, 1751–1758.

Maricq, M., & Xu, N. (2004). The effective density and fractal dimension of soot particles from premixed flames and motor vehicle exhaust. *Journal of Aerosol Science*, *35*, 1251–1274.

Maricq, M.M. (2007). Chemical characterization of particulate emissions from diesel engines: a review. *Journal of Aerosol Science*, *38*, 1079–1118.

McMurry, P.C., Wang, X., Park, K., & Ehara, K. (2002). The relationship between mass and mobility for atmospheric particles: a new technique for measuring particle density. *Aerosol Science and Technology*, *36*, 227–238.

Messing, M., Svensson, C., Meuller, B., Deppert, K., Pagels, J., & Rissler, J. Gas-borne particles with tunable and highly controlled characteristics for nanotoxicology studies. *Nanotoxicology*, in press.

Mills, N.L., Törnqvist, H., Robinson, S.D., Gonzalez, M., Darnley, K., MacNee, W., Boon, N.A., Donalson, K., Blomberg, A., Sandström, T., & Newby, D.E. (2005). Diesel exhaust inhalation causes vascular dysfunction and impaired endogenous fibrinolysis: an explanation for the increased cardiovascular mortality associated with air pollution. *Circulation*, *112*, 3930–3936.

Mills, N.L., Tornqvist, H., Gonzalez, M.C., Vink, E., Robinson, S.D., Soderberg, S., Boon, N.A., Donaldson, K., Sandström, T., Blomberg, A., & Newby, D.E. (2007). Ischemic and thrombotic effects of dilute diesel-exhaust inhalation in men with coronary heart disease. *New England Journal of Medicine*, *357*, 1075–1082.

Morawska, L., Hofmann, W., Hitchins-Loveday, J., Swanson, C., & Mengersen, K. (2005). Experimental study of the deposition of combustion aerosols in the human respiratory tract. *Journal of Aerosol Science*, *36*, 939–957.

Mullins, J., & Williams, A. (1987). The optical properties of soot: a comparison between experimental and theoretical values. *Fuel*, *66*, 277–280.

NIST 1650b. (2006). *Standard Reference Material: Diesel Particulate Matter*. 〈https://www-s.nist.gov/srmors/view_detail.cfm?srm=1650b〉.

Ntziachristos, L., Giechaskiel, B., Ristimäki, J., & Keskinen, J. (2004). Use of a corona charger for the characterisation of automotive exhaust aerosol. *Journal of Aerosol Science*, *35*, 943–963.

Olfert, J.S., Symonds, J.P.R., & Collings, N. (2007). The effective density and fractal dimension of particles emitted from a light-duty diesel vehicle with a diesel oxidation catalyst. *Aerosol Science*, *38*, 69–82.

Pagels, J., Khalizov, A.F., McMurry, P.H., & Zhang, R.Y. (2009). Processing of soot by controlled sulphuric acid and water condensation mass and mobility relationship. *Aerosol Science and Technology*, *43*, 629–640.

Park, K., Cao, F., Kittelson, D.B., & McMurry, P.H. (2003). Relationship between particle mass and mobility for diesel exhaust particles. *Environmental Science & Technology*, *37*, 577–583.

Park, K., Kittelson, D.B., Zachariah, M.R., & McMurry, P.H. (2004). Measurement of inherent material density of nanoparticle agglomerates. *Journal of Nanoparticle Research*, *6*, 267–272.

Pope, C.A., & Dockery, D.W. (2006). Health effects of fine particulate air pollution: lines that connect. *Journal of the Air & Waste Management Association*, *56*, 709–742.

Rissler, J., Pagels, J., Swietlicki, E., Wierzbicka, A., Strand, M., Lillieblad, L., Sanati, M., & Bohgard, M. (2005). Hygroscopic behavior of aerosol particles emitted from biomass fired grate boilers. *Aerosol Science and Technology*, *39*, 919–930.

Rissler, J., Vestin, A., Swietlicki, E., Fisch, G., Zhou, J., Artaxo, P., & Andreae, M.O. (2006). Size distribution and hygroscopic properties of aerosol particles from dry-season biomass burning in Amazonia. *Atmospheric Chemistry and Physics*, *6*, 471–491.

Rissler, J., Malik, A., Pagels, J., Messing, M., Nordin, E., Nilsson, P., Sanati, M., & Bohgard, M. On-line particle effective density measurements of several combustion aerosols using the DMA–APM system. *Journal of Aerosol Science*, submitted for publication.

Rothenbacher, S., Messerer, A., & Kasper, G. (2008). Fragmentation and bond strength of airborne diesel soot agglomerates. *Particle and Fibre Toxicology*, *5*, 9.

Sakurai, H., Tobias, H.J., Park, K., Zarling, D., Docherty, K.S., Kittelson, D.B., McMurry, P.H., & Ziemann, P.J. (2003a). On-line measurements of diesel nanoparticle composition and volatility. *Journal of Aerosol Science*, *37*, 1199–1210.

Sakurai, H., Park, K., McMurry, P.H., Zarling, D.D., Kittelson, D.B., & Ziemann, P.J. (2003b). Size-dependent mixing characteristics of volatile and nonvolatile components in diesel exhaust aerosols. *Environmental Science & Technology*, *37*, 5487–5495.

Salvi, S., Blomberg, A., Rudell, B., Kelly, F.J., Sandström, T., Holgate, S.T., & Frew, A.J. (1999). Acute inflammatory response in the airways and peripheral blood following short term exposure to diesel exhaust in healthy human volunteers. *American Journal of Respiratory and Critical Care Medicine*, *159*, 702–709.

Scheckman, J.H., & McMurry, P.H. (2011). Deposition of silica agglomerates in cast of human lung airways: enhancement relative to spheres of equal mobility and aerodynamic diameter. *Journal of Aerosol Science*, *42*, 508–516.

Schmid, O., Bolle, I., Harder, V., Karg, E., Takenaka, S., Schulz, H., & Ferron, G. (2008). Model for the deposition of aerosol particles in the respiratory tract of the rat. I. Nonhygroscopic particle deposition. *Journal of Aerosol Medicine and Pulmonary Drug Delivery*, *21*, 291–307.

Sehlstedt, M., Behndig, A., Boman, C., Blomberg, A., Sandström, T., & Pourazar, J. (2010). Airway inflammatory response to diesel exhaust generated at urban cycle running conditions. *Inhalation Toxicology*, *22*, 1144–1150.

Sorensen, C.M. (2011). The mobility of fractal aggregates: a review. *Aerosol Science and Technology*, *45*, 765–779.

Sydbom, A., Blomberg, A., Parnia, S., Stenfors, N., Sandstrom, T., & Dahlen, S.E. (2001). Health effects of diesel exhaust emissions. *European Respiratory Journal*, *17*, 733–746.

Törnqvist, H., Mills, N.L., Gonzalez, M., Robinson, S.D., Boon, N.A., MacNee, W., Donaldson, K., Söderberg, S., Newby, D.E., Sandström, T., & Blomberg, A. (2007). Persistent endothelial dysfunction in human subjects following diesel exhaust inhalation. *American Journal of Respiratory and Critical Care Medicine*, *15*, 395–400.

Tu, K.W., & Knutson, E.O. (1984). Total deposition of ultrafine hydrophobic and hygroscopic aerosols in the human respiratory system. *Aerosol Science and Technology*, *3*, 453–465.

Wang, C.-S., & Friedlander, S.K. (2007). Determination of surface area and volume of nanoparticle aggregates deposited in the human respiratory tract using DMA data. *Journal of Aerosol Science*, *38*, 980–987.

Weingartner, E., Burtscher, H., & Baltensperger, U. (1997). Hygroscopic properties of carbon and diesel soot particles. *Atmospheric Environment*, *31*, 2311–2327.

Weingartner, E., Gysel, M., & Baltensperger, U. (2002). Hygroscopicity of aerosol particles at low temperatures. 1. New low-temperature H-TDMA instrument: setup and first applications. *Environmental Science & Technology*, *36*, 55–62.

Wierzbicka, A., Lillieblad, L., Pagels, J., Strand, M., Gudmundsson, A., Gharibi, A., Swietlicki, E., Sanati, M., & Bohgard, M. (2005). Particle emissions from district heating units operating on three commonly used biofuels. *Atmospheric Environment*, *39*, 139–150.

Zelenyuk, A., & Imre, D. (2007). On the effect of particle alignment in the DMA. *Aerosol Science and Technology*, *41*, 112–124.